Tribology and Materials
Vol. x, No. x, 202x, pp. xx-xx

ISSN 2812-9717
https://doi.org/10.46793/tribomat.202x.xxx

Analysis of the axial force calculation method for turbocharger thrust bearing design

Vladislav HUDYAKOV, Elena ZADOROZHNAYA*

South Ural State University, Chelyabinsk, Russia
*Corresponding author: zadorozhnaiaea@susu.ru

Keywords
thrust bearing
axial force
turbocharger
hydromechanical
characteristics

History
Received: 28-09-2025
Revised: 21-12-2025
Accepted: 10-02-2026

Abstract

Turbochargers play a key role in increasing the performance and efficiency of modern internal combustion engines. However, their increased performance leads to an increase in mechanical loads, both in the radial and axial directions. This article examines modern methods for calculating the axial load on a turbocharger thrust bearing to optimise tribounit design and improve its hydromechanical characteristics. For this purpose, the analytical method of the control volume and numerical modelling in the Ansys Fluent software package, as well as software developed by the authors, were used. Based on the results of the study, an assessment of the applicability of these methods was performed, parametric calculations of the bearing design were carried out and the most effective geometric shape was determined.

1. Introduction

One of the most important components of a modern internal combustion engine is a turbocharger, which allows for increased power and fuel efficiency, as well as reduced engine weight and dimensions [1-3]. Modern consumer demands dictate trends in improving the design of a turbocharger in order to increase its efficiency, environmental friendliness, reliability of its elements and expand the operating ranges of the turbo unit [4-7].

Particular attention is paid to the selection of materials for turbocharger components, which are subject to existing thermal and mechanical loads. Turbine wheels, operating under extreme temperature conditions, are often made of heat-resistant nickel alloys, providing strength, temperature resistance and oxidation resistance. To reduce weight, turbine impellers are constructed of titanium-aluminium alloys. The compressor wheel is made of titanium alloys, ensuring low weight and high strength. The rotor, which experiences enormous torque and rotational speed, is made of high-strength heat-treated alloys. Bearings serve as support assemblies made of bronze alloys that provide antifriction properties [8,9].

Journal bearings, as support units of a turbocharger, have a direct impact on its reliability, durability and performance. The operation of journal bearings directly affects one of the most important indicators of turbocharger efficiency, namely, mechanical efficiency [10]. The design of tribounits should not only withstand the axial and radial loads that occur during operation but also ensure optimal values of friction losses [11,12]. In turn, the hydrodynamic thrust bearing should be given special attention, since friction losses in it can amount to a third of the total friction losses in the turbocharger bearings, even without applying an axial load [13].

The impact of the thrust bearing in the turbocharger rotor system significantly affects the trajectories of motion and the magnitude of the rotor oscillation amplitude. The difference in peak amplitude values, according to Mutra et al. [14], can reach 32 %. The performance characteristics of the thrust bearing are significantly affected by the purity and quality of the lubricant, as well as the lubricant supply pressure. Low quality of engine oil leads to a decrease in lubricating properties, failure

of the oil wedge and premature wear of bearing contact surfaces. In turn, insufficient lubricant supply pressure increases friction losses and wear [15]. The wear of the thrust bearing is also noticeably affected by the values of axial loads from the turbine and compressor.

Depending on the turbocharger's operating conditions, the direction of the axial load on the rotor changes. It can be directed toward the compressor or the turbine. Dynamic shock loads caused by combustion products can significantly impact system performance if the direction of the axial load changes [16]. Variable operating conditions, combined with high pressure on both sides of the turbocharger, create excessive thrust loading, which can lead to thrust bearing and turbocharger failure [17]. Thus, the axial load acting on the rotor has a significant impact on the service life of the turbocharger, its operating efficiency and the stability of its operation over a wide range of conditions.

Methods for assessing the axial forces acting on the thrust bearing of the turbojet engine are the subject of many works, which offer various analytical, experimental and numerical approaches. The research of Lee et al. [18] presents an analytical and experimental study for predicting the axial load acting on the thrust bearing of a turbojet engine. To determine the axial force, the thrust bearing deformation was measured on a test bench at each load value. In this case, not only the mechanical deformation of the bearing was considered, but also its thermal deformation. The authors plan to use the results of the study to optimise the design of the tribounit in order to reduce mechanical friction losses and improve the energy efficiency of the turbo unit.

The research of Wang et al. [19] is devoted to a new experimental technique for measuring the axial load acting on the rotor. Measurements are carried out using a force sensor, which eliminates problems of measurement repeatability or zero displacement. The experimental results were compared with numerical modelling data, and the measurement error did not exceed 8.17 %. The authors found that, at the same speed, the axial load of the compressor increases with decreasing mass flow, and the axial load on the turbine increases with increasing mass flow. In this case, the most loaded areas are the rear surface of the disc and the hub of the impellers, which is confirmed by Gjika and LaRue [20].

The study by Tiainen et al. [21] presents a comparison of various analytical methods for estimating the axial load acting on the compressor with the results of numerical modelling and experiment. The authors note that the results of numerical modelling underestimate the axial force by 26 – 58 %. Analytical methods often provide a large error in estimating axial force and require data that are not available at the initial stages of turbo unit design. To estimate the axial force acting on the compressor rotor, the authors propose a hybrid method that shows an error of no more than 13 %, compared to the experiment.

Based on a review of the scientific literature, there is a shortage of published papers devoted to the determination of axial load and comparative analysis of the results obtained using different methods. The purpose of this work is to evaluate the methods for determining the axial load acting on the turbocharger thrust bearing and to select the most optimal tribounits design to achieve the best hydromechanical characteristics. The novelty of this article lies in the comparison of analytical and numerical methods for calculating the axial force acting on the turbocharger rotor, as well as in the practical application of these data in optimising the geometry of the thrust bearing.

2. Numerical method for determining gas-dynamic axial forces

One of the reasons for this investigation is the failure of the turbocharger thrust bearing, shown in Figure 1. The object of the study is the turbocharger TKR 11N3 (D-160), developed by the Chelyabinsk Automobile and Tractor factory. Its appearance is shown in Figure 2. The diameter of the turbine wheel is 160 mm and the diameter of the compressor wheel is 170 mm. The operating mode under consideration corresponds to a rotor speed of 50,500 rpm.

Figure 1. Worn thrust bearing

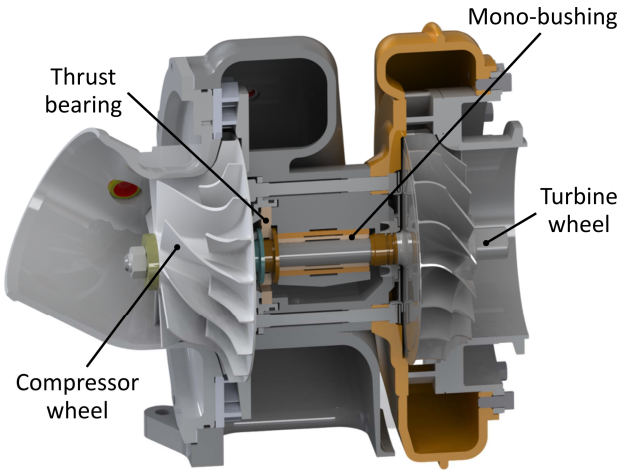

Figure 2. Visual appearance of the turbocharger TKR 11N3 (D-160)

To calculate the gas-dynamic forces, unstructured tetrahedral grid models were generated for the compressor and turbine (Fig. 3). The length of the inlet and outlet channels was increased by 8 characteristic diameters to ensure a fully developed and stable flow in the design domain. The number of cells varied from 9.4 million to 10.5 million. The maximum cell size did not exceed 9.8 mm, and the minimum was 0.003 mm. The convergence criteria were changes in pressure and temperature at the points. Dry air and exhaust gases for the compressor and turbine, respectively, were considered as working substances. The properties of these substances are given in Tables 1 and 2.

Table 1. Physical properties of exhaust gases; reprinted from Zadorozhnaya et al. [22], licensed under CC BY-NC 4.0

Temperature, °C	Density, kg/m^3	Heat capacity, J/kgK	Thermal conductivity, W/mK	Dynamic viscosity, Pas
273	1.295	1042	0.0228	1.58×10^{-5}
373	0.950	1068	0.0313	2.04×10^{-5}
473	0.748	1097	0.0401	2.45×10^{-5}
573	0.617	1122	0.0484	2.82×10^{-5}
673	0.525	1151	0.0570	3.17×10^{-5}
773	0.457	1185	0.0656	3.48×10^{-5}
873	0.405	1214	0.0742	3.79×10^{-5}
973	0.363	1239	0.0827	4.07×10^{-5}

Table 2. Physical properties of dry air; reprinted from Zadorozhnaya et al. [22], licensed under CC BY-NC 4.0

Temperature, °C	Density, kg/m^3	Heat capacity, J/kgK	Thermal conductivity, W/mK	Dynamic viscosity, Pas
273	1.293	1005	0.0244	1.72×10^{-5}
373	0.946	1009	0.0321	2.19×10^{-5}
473	0.746	1026	0.0393	2.60×10^{-5}
573	0.615	1047	0.0460	2.97×10^{-5}
673	0.524	1068	0.0521	3.30×10^{-5}
773	0.456	1093	0.0574	3.62×10^{-5}
873	0.404	1114	0.0622	3.91×10^{-5}
973	0.362	1135	0.0671	4.18×10^{-5}

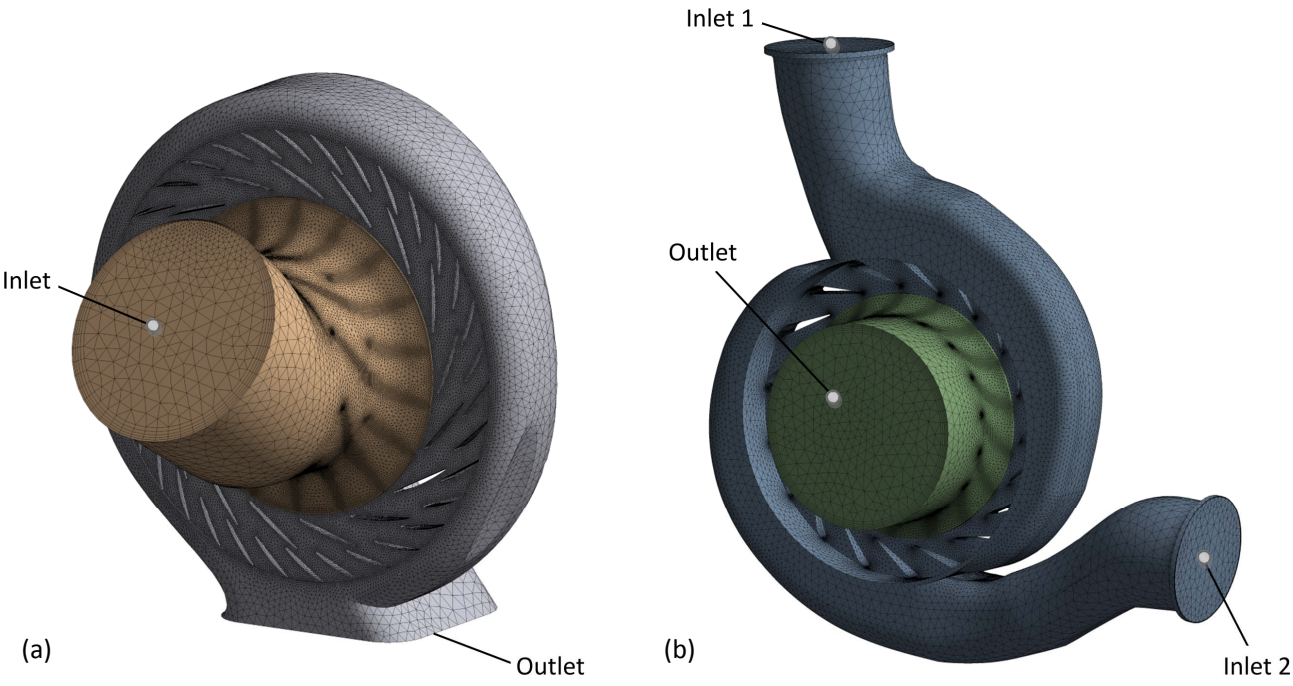

Figure 3. Calculation mesh model: (a) compressor and (b) turbine

The simulation was performed in the commercial software package Ansys Fluent. The flow rate at the turbine inlet boundary was set to 0.7225 kg/s, and the pressure at the outlet boundary was set to 101 kPa. The exhaust gas temperature in the casing was equivalent to 678 K. The pressure at the compressor inlet boundary was set to 101 kPa and the temperature to 293 K. The pressure at the outlet boundary was set to 225 kPa and the temperature to 458 K. The influence of roughness in the calculation of gas-dynamic forces was not taken into account. The solver settings and the choice of physical models are described in the author's previous work [22].

3. Analytical method for determining gas-dynamic axial forces

For the analytical calculation of the axial forces acting on the turbocharger rotor, the control volume method proposed by Nguyen-Schäfer [23] was used. The method shows good agreement with the results of the numerical calculation, and the error of the results is less than 10%. From the assumptions, it can be noted that the flow is stationary, and the viscosity on the walls of the control volume is negligible. According to the method, the axial force acting on the compressor wheel can be divided into four components $F_{1,C}$, $F_{2,C}$, $F_{3,C}$ and $F_{4,C}$ (Fig. 4).

The force acting on the inlet surface of the compressor wheel is expressed as:

$$F_{1,C} = A_1 p_1 = \frac{\pi p_1 D_1^2}{4}, \quad (1)$$

where A_1 is the compressor inlet cross-sectional area, p_1 is the inlet pressure of the ambient air and D_1 is the inflow diameter of the compressor.

The pressure force at the shroud surface can be represented by the following expression:

$$F_{2,C} = A_S \left(\frac{p_1 + p_{2*}}{2} \right) = \frac{\pi (D_2^2 - D_1^2)(p_1 + p_{2*})}{8}, \quad (2)$$

where A_S is the projected area of the shroud surface in the axial direction, p_{2*} is the compressor outlet pressure and D_2 is the compressor outlet diameter.

The impulse force acting on the surface of the compressor wheel is expressed as follows:

$$F_{3,C} = \frac{Q_{mC} R T_1}{A_1 p_1}, \quad (3)$$

where Q_{mC} is the mass flow, R is the gas constant and T_1 is the compressor inlet air temperature.

The force acting on the back surface of the compressor wheel is calculated as:

$$F_{4,C} = A_{bf,C}\, p_{2*} = \frac{\pi (D_2^2 - D_{rotor}^2)}{4} p_{2*}, \quad (4)$$

where $A_{bf,C}$ is the compressor back-face surface area and D_{rotor} is the rotor diameter.

The resulting force acting on the compressor wheel is expressed as follows:

$$F_{CW} = F_{1,C} + F_{2,C} + F_{3,C} - F_{4,C}. \quad (5)$$

The force acting on the turbine wheel is calculated in a similar manner:

$$F_{TW} = -F_{1,T} - F_{2,T} - F_{3,T} + F_{4,T}. \quad (6)$$

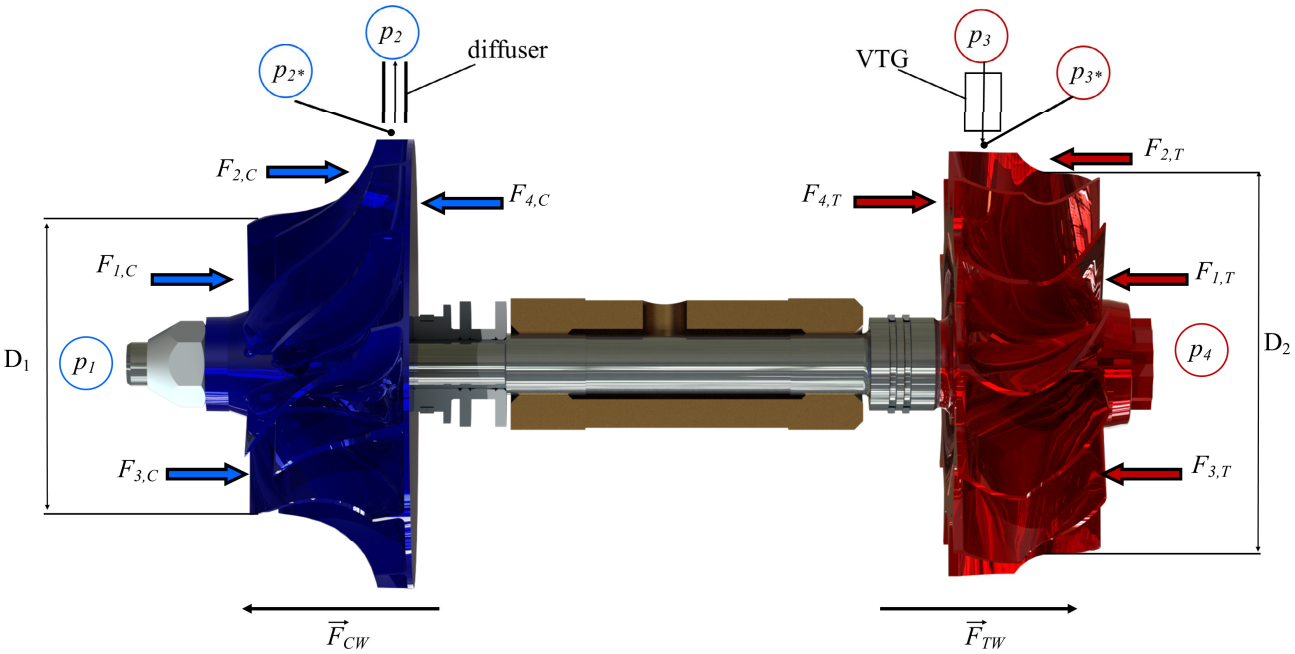

Figure 4. Axial forces acting on the turbocharger rotor

The axial force acting on the turbocharger rotor is defined as:

$$F_{T,ax} = F_{CW} + F_{TW}. \quad (7)$$

The total value of the axial force acting on the TCR rotor was −1449 N. The negative value indicates the predominance of the force from the turbine. The results of the analytical calculation of the axial force components are given in Table 3.

Table 3. Values of the axial force components

Impeller	F_1, N	F_2, N	F_3, N	F_4, N	F, N	$F_{T,ax}$, N
Turbine	1450	2755	18.3	6394	2171	−7292
Compressor	1449	1108	2518	45.4	−3620	

4. Parametric study of thrust bearing design

The calculation was performed in a quasi-static formulation using the software developed by Tiainen et al. [24]. The calculation principle consists of a gradual decrease in the initial clearance of the thrust bearing and the determination of the bearing capacity, which is compared with the calculated axial load. In this case, the hydromechanical characteristics of the tribounit were determined: lubricant layer temperature, lubricant consumption in the radial and circumferential directions, friction losses and maximum hydrodynamic pressure.

The calculation was stopped when the bearing capacity and the specified axial load were equal or when the minimum difference between them was reached. The working surface is formed by 6 pads with working platforms separated by radial grooves. Each pad contains an inclined (with a coverage angle of θ_1) and horizontal (with a coverage angle of θ_2) part. The full coverage of the pad θ varied from 49 to 54 degrees. The block diagram is shown in Figure 5. The angle of the inclined block was taken to be 20'. The inner radius r_1 = 11.7 mm and the outer radius r_2 = 19 mm.

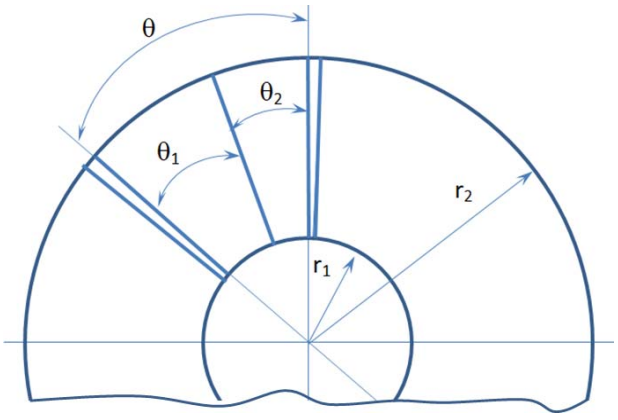

Figure 5. Thrust bearing pad design

The following input parameters were used in the study. The rotor speed was 50,500 rpm, the excess oil supply pressure was 0.5 MPa and the supply temperature was 90 °C. SAE 5W-40 engine oil was used as the working fluid. The design options for the pads that were considered in the study are shown in Table 4.

Table 4. Thrust bearing design options for calculation

Option	Pad coverage angle θ, °	Groove width at average radius, mm	Ratio $\delta = \theta/\theta_2$
1	49.230	10.770	2
2			2.5
3			3
4			3.5
5	52.470	7.530	2
6			2.5
7			3
8			3.5
9	54.615	5.385	2
10			2.5
11			3
12			3.5

The following assumptions were made when conducting numerical studies:

- the lubricant flow regime is laminar,
- lubricant particles at the boundary with the solid body have a velocity corresponding to a point on the body,
- radial movement of the pad is not taken into account,
- pressure across the thickness of the lubricant layer is assumed to be constant,
- hydrodynamic reaction of the lubricant layer is directed normal to the pad surface,
- due to the symmetry of the problem, the pressure fields were determined for a single segment of the thrust bearing,
- thrust bearing segments are assumed to be stationary, the tangential dimension of the thrust bearing segment L is equal to the arc of the average radius and the width is $b = r_2 - r_1$,
- inertial forces of the lubricating layer are not taken into account.

An isothermal approach was used to assess the thermal state of the bearing. The hydrodynamic pressure field $p(x, z)$ in the lubricating layer of a non-Newtonian fluid is

determined by integrating the generalised Reynolds equation. The finite difference method was used to solve the Reynolds equation, ensuring the accuracy of the solution at pressure convergence orders up to $\varepsilon = 10^{-5}$. The number of points in each element was 47 × 89.

The pressure task can be solved using various iterative methods. A simple and flexible algorithm that takes into account bearing geometry and inequality conditions is the Seidel algorithm [25]. The iterative process for finding the pressure distribution stops when the convergence condition is met:

$$\left|\frac{\sum\sum(p_{ij}^{\rho+1}-p_{ij}^{\rho})}{\sum\sum p_{ij}^{\rho}}\right| \le \varepsilon, \qquad (8)$$

where ρ is the iteration number.

5. Results and discussion

As a result of the calculations, values of axial force were obtained and compared with data presented in studies by other authors. A comparison of axial force values acting on the thrust bearing is given in Table 5.

As can be seen from the presented results, the values of the axial force vary significantly depending on the selected calculation method, operating mode and turbocharger dimension. In this case, a fivefold difference is noticed between the results of the analytical and numerical methods. Some authors noted that the analytical control volume method predicts axial force well at low rotation speeds and in the absence of leaks. Otherwise, the value may differ by 50 – 85 %. The Nguyen-Schäfer method also assumes constant pressure in the area behind the rear surface of the impeller, which is not confirmed by numerical calculations and data from the works of other authors [18]. This assumption leads to overestimated values of the pressure on the rear surface of the impeller and the axial force. The absence of consideration of viscous forces in the control volume method has an insignificant effect on the axial force assessment, since the magnitude of these forces is no more than 2.5 % of the total value. Thus, it can be concluded that the analytical method of the control volume is acceptable for use, but it should be taken into account that it overestimates the axial force many times, and there is not enough experimental data for a full comparison.

Based on the value of the calculated axial reaction

$$R = \int_{r_1}^{r_2}\int_{0}^{L} p(x,z)\mathrm{d}x\mathrm{d}z,$$

we can proceed to the results of modelling the turbocharger thrust bearing. As a result of the axial bearing calculation, the following hydromechanical parameter values were obtained: load-bearing capacity, lubricant layer temperature, friction losses, oil flow rate and maximum pressure.

For comparison of variants with different pad coverage angles θ, the results are presented in Table 6. With an increase in the pad coverage angle, the load-bearing capacity increases. At the same time, friction losses increase by 6 – 11 %. The highest load-bearing capacity is achieved with a coverage angle of 49.23 and a ratio of δ = 3. The minimum permissible clearance in all variants is equivalent to 9 μm, after which a "breakdown" of the load-bearing capacity is noticed. To withstand the analytically calculated axial load, a clearance of 17 – 18 μm is required. To withstand the numerically determined load, a clearance greater than 50 μm is required. A comparison of the load-bearing capacity of the thrust bearing depending on the size of the clearance with axial forces obtained by different methods is shown in Figure 6.

Table 5. Comparison of axial force values acting on a thrust bearing

Reference	Rotation speed, rpm	Wheels diameter, mm	Axial force, N		
			Analytical method	Numerical method	Experiment
Wang et al. [19]	90,000	84 – 93	–	183	200
Thiyagarajan et al. [26]	1200	–	– 60	–	– 83
Mishra and Behera [27]	100,000	96 – 102	– 4540	–	–
Dadaev [28]	24,000	–	–	280	289
Current research	50,500	160 – 170	– 1449	– 244	–

Table 6. Calculation results with different pad coverage angle θ

Option	Minimum permissible clearance, μm	Load-bearing capacity, N	Lubricant layer temperature, °C	Friction losses, W	Oil flow rate, m^3/s	Maximum pressure, MPa	Pad coverage angle θ, °
1	9	3640	122.8	5363	1.06×10^{-2}	77.4	49.230
2		3881	121.6	5342	1.10×10^{-2}	154	
3		3938	119.8	5268	1.15×10^{-2}	242	
4		3881	121.6	5342	1.10×10^{-2}	154	
5		3684	123.6	5735	1.11×10^{-2}	91.3	52.470
6		3867	122.1	5713	1.16×10^{-2}	199	
7		3888	119.5	5487	1.21×10^{-2}	270	
8		3837	116.9	5199	1.26×10^{-2}	262	
9		3698	124.2	5989	1.14×10^{-2}	102	54.615
10		3838	122.2	5942	1.20×10^{-2}	226	
11		3825	119.2	5666	1.26×10^{-2}	264	
12		3753	116.0	5229	1.30×10^{-2}	226	

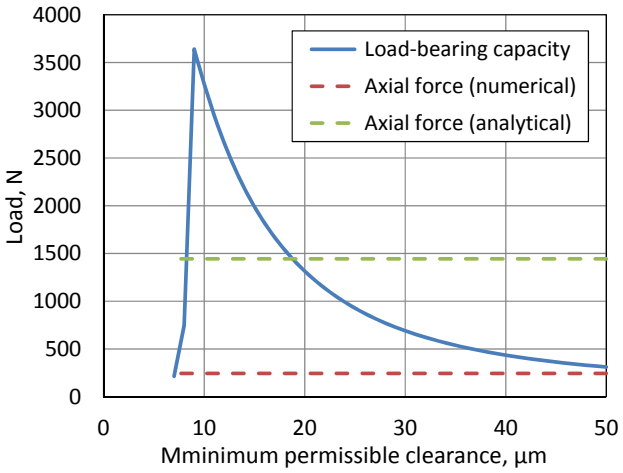

Figure 6. Load-bearing capacity of thrust bearing as a function of minimum permissible clearance and comparison with axial forces obtained by different methods

In this figure, the blue line shows the change in load-bearing capacity as the lubricant film thickness changes. Upon reaching a thickness of 8 μm, a sharp drop in load-bearing capacity is observed. The yellow and orange lines show the axial force values calculated using analytical and numerical methods to determine the required clearance for bearing operation at rotation speeds of 50 – 500 rpm.

6. Conclusion

This paper presents a study of the evaluation of methods for determining the axial load acting on the turbocharger thrust bearing, as well as the results of selecting the optimal tribounit design to achieve the best hydromechanical characteristics.

Based on the results, it can be concluded that there is a significant difference between the data obtained by the analytical method and that obtained by 3D numerical modelling. The analytical method of the control volume developed by Nguyen-Schäfer is acceptable since it is simpler and faster in estimating the axial load, but due to a number of assumptions, it can significantly overestimate it. For a full comparison of the adequacy of the methods, there is not enough experimental data. In addition, in the scientific literature, no sources were found that included all the specified research methods. Furthermore, analysis of other authors' work confirmed a wide range of values for the axial force acting on the rotor, making it difficult to assess the accuracy of a specific method without experimental studies for the selected turbocharger model.

Parametric studies of the turbocharger thrust bearing revealed the following dependencies. With an increase in the pad coverage angle, the load-bearing capacity increases. Friction losses also increase by 6 – 11 %. The highest load-bearing capacity is achieved with a coverage angle of 49.23 and a ratio of full and horizontal coverage (δ ratio) of 3. The minimum permissible clearance in all considered variants is equivalent to 9 μm, after which a "breakdown" of the load-bearing capacity is noticed.

Further research is planned to be devoted to the influence of the thrust bearing on the dynamics of the turbocharger rotor, as well as to the assessment of changes in its hydromechanical characteristics due to skew.

Acknowledgement

The work was carried out with the financial support of the Russian Foundation for Basic Research (project No. 20-48-740007\20).

References

[1] R.G. Kirk, A.A. Alsaeed, E.J. Gunter, Stability analysis of a high-speed automotive turbocharger, Tribology Transactions, Vol. 50, No. 3, 2007, pp. 427-434, DOI: 10.1080/10402000701476908

[2] J. Yang, Y. Gao, Z. Liu, C. Zhao, T. Kang, L. Gu, B. Xu, A method for modeling and analyzing the rotor dynamics of a locomotive turbocharger, Nonlinear Dynamics, Vol. 84, No. 1, 2016, pp. 287-293, DOI: 10.1007/s11071-015-2497-z

[3] L. Wang, G. Bin, X. Li, X. Zhang, Effects of floating ring bearing manufacturing tolerance clearances on the dynamic characteristics for turbocharger, Chinese Journal of Mechanical Engineering, Vol. 28, No. 3, 2015, pp. 530-540, DOI: 10.3901/CJME.2015.0319.034

[4] A.J. Feneley, A. Pesiridis, A.M. Andwari, Variable geometry turbocharger technologies for exhaust energy recovery and boosting – A review, Renewable and Sustainable Energy Reviews, Vol. 71, 2017, pp. 959-975, DOI: 10.1016/j.rser.2016.12.125

[5] G. Ying, G. Meng, J. Jing, Turbocharger rotor dynamics with foundation excitation, Archive of Applied Mechanics, Vol. 79, No. 4, 2009, pp. 287-299, DOI: 10.1007/s00419-008-0228-3

[6] Z. Cao, H. Guo, Z. Cheng, R. Men, Z. Zhang, T. Wang, Nonlinear dynamics characteristics of a tilting pad journal bearing supported turbocharger, Nonlinear Dynamics, Vol. 112, No. 19, 2024, pp. 16941-16961, DOI: 10.1007/s11071-024-09948-3

[7] Y. Zhang, W. Wang, D. Wei, G. Wang, J. Xu, K. Liu, Dynamic stability of unbalance-induced vibration in a turbocharger rotor-bearing system with the nonlinear effect of thermal turbulent lubricating fluid film, Journal of Sound and Vibration, Vol. 528, 2022, Paper 116909, DOI: 10.1016/j.jsv.2022.116909

[8] G. Gudivada, A.K. Pandey, Recent developments in nickel-based superalloys for gas turbine applications: Review, Journal of Alloys and Compounds, Vol. 963, 2023, Paper 171128, DOI: 10.1016/j.jallcom.2023.171128

[9] T.H. Danh, L.H. Ky, P.H. Anh, D.T. Tam, N.H. Hiep, Evaluation strength of materials of the compressor wheel and engine power in the turbocharger, Engineering, Technology & Applied Science Research, Vol. 14, No. 4, 2024, pp. 15734-15738, DOI: 10.48084/etasr.7891

[10] P. Novotný, J. Hrabovský, Efficient computational modelling of low loaded bearings of turbocharger rotors, International Journal of Mechanical Sciences, Vol. 174, 2020, Paper 105505, DOI: 10.1016/j.ijmecsci.2020.105505

[11] A.M. Elzahaby, S.A. El-Agouz, A.F. Nemnem, A.A. Mubarak, Investigation of the axial rotor thrust in centrifugal compressors, Journal of Engineering Research, Vol. 3, No. 3, 2019, pp. 11-18.

[12] V.M. Koufopanos, A. Andrikopoulos, P. Nikolakopoulos, Power losses vs. mechanical load of an active magnetic bearing: A finite element method approach, Tribology and Materials, Vol. 4, No. 2, 2025, pp. 90-99, DOI: 10.46793/tribomat.2025.011

[13] B. Lüddecke, P. Nitschke, M. Dietrich, D. Filsinger, M. Bargende, Unsteady thrust force loading of a turbocharger rotor during engine operation, Journal of Engineering for Gas Turbines and Power, Vol. 138, No. 1, 2016, Paper 012301, DOI: 10.1115/1.4031142

[14] R.R. Mutra, J. Srinivas, D. Mallikarjuna Reddy, M.N.A. Rani, M.A. Yunus, Z. Yahya, Dynamic and stability comparison analysis of the high-speed turbocharger rotor system with and without thrust bearing via machine learning schemes, Journal of the Brazilian Society of Mechanical Sciences and Engineering, Vol. 46, No. 5, 2024, Paper 316, DOI: 10.1007/s40430-024-04892-0

[15] T. Dziubak, M. Karczewski, Operational malfunctions of turbochargers – reasons and consequences, Combustion Engines, Vol. 164, No. 1, 2016, pp. 13-21, DOI: 10.19206/CE-116484

[16] R.R. Mutra, A. Mhatre, J. Srinivas, B. Venkateswarlu, D. Mallikarjuna Reddy, Investigation and parametric studies of turbocharger rotor bearing system behavior with a thrust bearing, AIP Conference Proceedings, Vol. 2545, No. 1, 2022, Paper 020001, DOI: 10.1063/5.0103275

[17] J. Zhang, H. Sun, L. Hu, H. He, Fault diagnosis and failure prediction by thrust load analysis for a turbocharger thrust bearing, in Proceedings of the ASME 2010 Turbo Expo: Turbine Technical Conference and Exposition, Volume 6, 14-18.06.2010, Glasgow, UK, pp. 491-498, DOI: 10.1115/GT2010-22320

[18] I. Lee, S. Hong, Y. Kim, B. Choi, Prediction of axial thrust load under turbocharger operating conditions, Transactions of the Korean Society of Automotive Engineers, Vol. 24, No. 6, 2016, pp. 642-648, DOI: 10.7467/KSAE.2016.24.6.642

[19] C. Wang, R. Yan, Z. Ding, D. Tong, X. Wu, C. Gao, L. Zhuang, 涡轮增压器轴向力变化规律试验与仿真 [Experimental and simulation study on axial

force variation of turbocharger], Acta Armamentarii, Vol. 44, No. 1, 2023, pp. 307-315, DOI: 10.12382/bgxb.2022.0045 [in Chinese].

[20] K. Gjika, G.D. LaRue, Axial load control on high-speed turbochargers: Test and prediction, in Proceedings of the ASME 2008 Turbo Expo: Turbine Technical Conference and Exposition, Volume 1, 09-13.06.2008, Berlin, Germany, pp. 705-712, DOI: 10.1115/GT2008-50756

[21] J. Tiainen, A. Jaatinen-Värri, A. Grönman, P. Sallinen, J. Honkatukia, T. Hartikainen, Validation of the axial thrust estimation method for radial turbomachines, International Journal of Rotating Machinery, Vol. 2021, 2021, Paper 6669193, DOI: 10.1155/2021/6669193

[22] E. Zadorozhnaya, V. Hudyakov, S. Sibiryakov, Simulation of heat transfer in a turbocharger bearing housing, Tribology and Materials, Vol. 1, No. 2, 2022, pp. 42-54, DOI: 10.46793/tribomat.2022.007

[23] H. Nguyen-Schäfer, Rotordynamics of Automotive Turbochargers, Springer, Cham, 2015, DOI: 10.1007/978-3-319-17644-4

[24] Y. Rozhdestvensky, E. Zadorozhnaya, S. Cherneyko, Модель расчета упорного подшипника скольжения с лазерным текстурированием несущей поверхности [Mathematical model for calculating thrust bearing with laser texturing of bearing surface], Bulletin of the South Ural State University. Series: Mathematical Modelling, Programming & Computer Software, Vol. 8, No. 1, 2015, pp. 5-23, DOI: 10.14529/mmp150101 [in Russian].

[25] R. Barrett, M. Berry, T.F. Chan, J. Demmel, J. Donato, J. Dongarra, V. Eijkhout, R. Pozo, C. Romine, H. van der Vorst, Templates for the Solution of Linear Systems: Building Blocks for Iterative Methods, SIAM, Philadelphia, 1994, DOI: 10.1137/1.9781611971538

[26] J. Thiyagarajan, E. Halldorf, J. Fridh, Transient thrust forces on a twin scroll turbocharger, in Proceedings of the ASME 2017 Turbo Expo: Turbine Technical Conference and Exposition, Volume 8, 26-30.06.2017, Charlotte, USA, Paper V008T26A009, DOI: 10.1115/GT2017-63658

[27] H.P. Mishra, S.K. Behera, Design of herringbone grooved thrust bearing for locomotive turbocharger rotor, Engineering Research Express, Vol. 6, No. 2, 2024, Paper 025558, DOI: 10.1088/2631-8695/ad5303

[28] S.G. Dadaev, Нестационарные модели газодинамических подшипников со спиральными канавками: Монография [Non-stationary models of gas-dynamic bearings with spiral grooves: Monograph], Publishing house SUSU, Chelyabinsk, 2000 [in Russian].